Magnetic nanocomposites based on phosphorus-containing polymers – structural characterization and thermal analysis

R. M. Alosmanov[a,b,*], M. Szuwarzyński[b,c], J. Schnelle-Kreis[d], G. Matuschek[d], A. M. Magerramov[a], A. A. Azizov[a], R. Zimmermann[d,e], S. Zapotoczny[b,*]

[a] Baku State University, Chemistry Department, Z. Khalilov str., 23, Baku, AZ1148 Azerbaijan

[b] Jagiellonian University, Faculty of Chemistry, Gronostajowa 2, 30-387 Krakow, Poland.

[c] AGH University of Science and Technology, Academic Centre for Materials and Nanotechnology, al. Mickiewicza 30, 30-059, Krakow, Poland

[d] Joint Mass Spectrometry Centre, Cooperation Group "Comprehensive Molecular Analytics", Helmholtz Zentrum München, German Research Center for Environmental Health (GmbH), Ingolstädter Landstraße 1, D-85764 Neuherberg, Germany

[e] Joint Mass Spectrometry Centre, Institute of Chemistry, University of Rostock, Rostock, Dr. Lorenz Weg 1, D-18051 Rostock, Germany

Corresponding authors: Szczepan Zapotoczny (email: zapotocz@chemia.uj.edu.pl), Rasim Alosmanov (r_alosmanov@rambler.ru)

Abstract

Fabrication of magnetic nanocomposites containing iron oxide nanoparticles formed *in situ* within a phosphorus-containing polymer matrix as well as its structural characterization and its thermal degradation is reported here. Comparative structural studies of the parent polymer and nanocomposites were performed using FTIR spectroscopy, X-ray diffraction, Atomic Force Microscopy. The results confirmed the presence of dispersed iron oxides magnetic

nanoparticles in the polymer matrix. The formed composite combines the properties of porous polymer carriers and the magnetic particles enabling easy separation and reapplication of such polymeric carriers used for e.g. catalysis or environmental remediation. Studies on thermal degradation of the composites revealed that the process proceeds in three stages while significant influence of the embedded magnetic particles on that process was observed in the first two stages. Magnetic Force Microscopy studies revealed that nanocomposite and its calcinated form have strong magnetic properties. The obtained results provide comprehensive characterization of the magnetic nanocomposites and the products of their calcination that are important for their possible applications as sorbents (regeneration conditions, processing temperature, disposal, etc.).

Keywords: Nanocomposites; Magnetic nanoparticles; Magnetic Force Microscopy; Thermal analysis

1. Introduction

Unique physical and chemical properties of nanoparticles (NPs) that are related to quantum size effects and large surface area/energy are the major factors influencing a growing interest in fundamental studies and applications of NPs [1,2,3]. While NPs have a strong tendency to agglomeration [4,5] there have been number of methods developed for their stabilization by using various materials, including inorganic compounds [6], surfactants [7] and polymers [8,9]. The incorporation of NPs in polymer or other matrices allow obtaining new nanocomposite materials [6−9]. Among the broad spectrum of such systems magnetic nanocomposites (MNCs) have gained significant attention due to their intrinsic magnetic properties [10−12]. Magnetic NPs due to their small size commonly exhibit superparamagnetic properties that make them useful as e.g. contrast agents in magnetic resonance imaging (MRI) [13,14], drug carriers [15,16] or in hyperthermia treatment [17].

MNCs combining magnetic properties of NPs and tunable porous structure and mechanical properties of the polymer matrix have been considered as desired materials for various application in e.g.: information technology, telecommunications [18,19], catalysis [20], MRI [13,21], biomedicine and environmental remediation [22−24]. Taking advantage of soft polymer matrices the nanocomposites with well-dispersed magnetic (nano)particles may be formed overcoming common difficulties related to their aggregation that often leads to diminishing their magnetic properties [25]. Therefore, designing and preparation of various magnetic nanostructures have been a subject of numerous studies [26,27].

MNCs can be generally prepared by either embedding of the preformed magnetic NPs in a soft polymer matrix or by their synthesis *in situ* within the porous polymer material using appropriate soluble precursors. Due to diffusion limits, synthesis of magnetic NPs from their soluble precursors in the polymer matrix seems to be favorable for reaching uniform distribution of NPs in MNC. Such composites may be obtained through the hydrolysis or reduction of metal salts in the presence of polymers [28,29]. Ziolo et al. developed a method to synthesize γ-Fe_2O_3 NPs in a commercial ion exchange resin [30]. For this purpose ion exchange of iron ions by the cross-linked sulfonated porous polystyrene was carried out followed by precipitation of iron oxide NPs in the polymer matrix. This method was then applied to obtain MNCs based on cross-linked polymers such as anions and cations exchangers [31−35] as well as macromolecular oxidizers [36] that have numerous environmental applications. For example, sorption properties of the synthesize MPCs for the oxyanions of arsenic [31], Cu^{2+}, Zn^{2+} [32], sulphide [33] were investigated.

Thermal analytical methods are widely used in the study of the relationship between the composition and processing temperature of materials as well as their thermal degradation. It is particularly important for materials used as sorbents. First of all, many processes involving such materials are carried out at relatively high temperatures and may be accompanied by some structural change of the sorbents. Moreover, characterization of the sorbent materials

using thermal methods is important for their regeneration or calcination (e.g. prior to disposal). Finally, if the sorption materials are polymeric composites, their thermal analysis allow to identify the impact of various components on the thermal stability of the polymer.

This paper presents the synthesis and thermal degradation of new MNCs based on phosphorus-containing polymer (PhCP). PhCP was applied as efficient sorbent of heavy metal ions [37] and formation of magnetic nanocomposites may be the way of their efficient separation from the environment without necessity of filtrations [38]. PhCP was synthesized by chemical modification (oxidative chlorophosphorylation reaction) of industrial polymer – butadiene rubber (BR). In this work structural characterization and thermal degradation (TD) of the PhCP and respective MNC based on PhCP were investigated. A kinetic analysis of the TD process by means of the Friedman and Ozawa-Flynn-Wall (OFW) kinetic methods was also presented.

2. Experimental

2.1. Materials

BR was purchased from Voronezh Synthetic Rubber Manufactory (Russia). PCl_3, CCl_4, p-xylene, $FeCl_2 \cdot 4H_2O$, $FeCl_3 \cdot 6H_2O$, NaOH (all p.a.) were supplied by Gorex Analyt GmbH and used without further purification. Oxygen was purified (removal of traces of water) by passing it through concentrated sulfuric acid (VI) (Gorex Analyt GmbH). All aqueous solutions used for the experiments were prepared using distilled water.

2.2. Synthesis of the phosphorus-containing polymer (PhCP)

The synthesis was realized following our previously reported method [39]. Namely, 5% solution of BR in CCl_4 was mixed with PCl_3 (BR:PCl_3, 1:5 w/w ratio). The reaction was carried out at room temperature for8 hours under the oxygen flow (7 $L \cdot h^{-1}$) and after its completion p-xylene was added to the reaction solution. Then, the liquid components (CCl_4,

$POCl_3$, unreacted PCl_3) were evaporated under intensive stirring using a vacuum pump leaving solid phosphochlorinated BR in the form of swollen powder (PChBR). This product was a cross-linked functional polymer (-$P(O)Cl_2$, phosphonyldichloride and -$OP(O)Cl_2$, phosphoryldichloride groups) with P-Cl bonds. Then the mixture of PChBR and p-xylene was added to ice water for separation of the cross-linked polymer. The separated polymer was subjected to hydrolysis that was carried out at 50°C for 4 h with continuous stirring. The product was filtered, washed with distilled water several times until neutral pH was reached. Then it was washed with acetone and dried in air and then under vacuum at 40°C. The final product (PhCP) was obtained in a form of dark-brown powder.

2.3. Synthesis of the magnetic nanocomposite (Ph-MNC) based on PhCP

The previously reported synthetic procedure was modified here [38]. Namely, ferric and ferrous chlorides (with a molar ratio 2:1) were dissolved in water with a total concentration of 0.1 M of iron ions. Then, the 100 mL the mixture of solutions of iron salts was added to the 1.0 g of PhCP. The suspension was stirred for 2h and then the polymer was filtered off, washed thoroughly with distilled water and dried in air. 2M solution of sodium hydroxide (100 mL) was added to the air-dried PhCP with Fe^{2+} and Fe^{3+} ions. The reaction was carried on for 1 h at 80°C under argon atmosphere with a constant and vigorous stirring. The obtained pure black Ph-MNC nanocomposite was separated using an external magnetic field (neodymium magnet) and was treated by 1M HCl solution for removal of the surface attached particles. Afterwards, Ph-MNC was washed several times with water and ethanol, separated *via* centrifugation and finally dried in a vacuum oven at 50°C. PhCP and Ph-MNC were scuffed in an agate vessel up to disperse state (35-50 mesh).

2.4. Characterization methods

For determination of the content of iron in Ph-MNC, the sample was treated with a mixture of concentrated HCl and HNO_3 (1:1) followed by appropriate dilution of the formed solution and analyzed using an atomic-emission spectrometer (Optima 2100 DV, Perkin-Elmer). XRD patterns of the Ph-MNC was recorded on an automatic diffractometer "D2 PHASER" (Bruker) at room temperature (Cu-Kα1, λ = 1.54060 Å). FTIR spectroscopy measurements were performed using a Thermo Nicolet iS10 FTIR spectrometer (Thermo Scientific) with ATR equipment (SMART iTX). The samples were vacuum dried before the measurements. Spectra were baseline corrected and normalized using Omnic v9.0 software (Thermo Scientific). Atomic Force Microscopy (AFM) images were obtained with Dimension Icon microscope (Bruker) working in air using Tapping Mode. Magnetic Force Microscopy (MFM) images were acquired using the same microscope working in the lift mode. In all measurements magnetic Co/Cr coated standard silicon cantilevers with nominal spring constant of 2 N/m were used. Before scanning the cantilevers were magnetized with a small magnet. All MFM images were taken within lift (surface-tip) distance of 100 nm.

Thermogravimetric analyses (TGA) were performed on NETZSCH TG 209/cell Thermal Analysis System between 20 and 850°C by the use of Al_2O_3 crucibles. The measurements were carried out under the flow of synthetic air (35 mL min^{-1}) at five different heating rates (β=1, 5, 10, 15 and 20 K min^{-1}) for granulated samples. The samples after the measurements (heated up to 850°C) were further investigated (calcinated samples).

3. Results and Discussion

In our previous studies PhCP materials were described in details [39]. According to the results of solid state ^{1}H, ^{13}C, and ^{31}P NMR analysis it was established that the PhCP contains phosphonate ($–P(O)(OH)_2$) and phosphate ($–OP(O)(OH)_2$) groups. Chlorine and hydroxyl groups directly connected to the carbon atoms of the main macromolecular chain: –CHCl; –CH(OH) are also present there. The presence of functional groups in the cross-linked PhCP as

well as its porous structure enables adsorption of iron ions and subsequent formation of magnetic particle in the polymer matrix leading to Ph-MNC (Fig.1, A–C). Such nanocomposites, thanks to the presence of magnetic particles, can be easily isolated from the suspension just by applying magnetic field (see Fig. 2). Such capability is very important for possible applications of PhPC-based materials in e.g. catalysis or environmental remediation. Structure and magnetic properties of the obtained Ph-MNC were investigated by FTIR and AFM-MFM techniques. Moreover, to study distribution of magnetic particles XRD analysis was performed. Additionally, parent PhCP polymer material and the obtained Ph-MNC nanocomposite were thermally treated (up to 850°C) using TGA (Fig. 1, A to D and C to E; In the real picture clearly visible as Ph-MNC (flask C) and its calcinated form CPh-MNC (flask E) has magnetic properties). FTIR, AFM-MFM measurements were performed for C-PhCP and CPh-MNC as well.

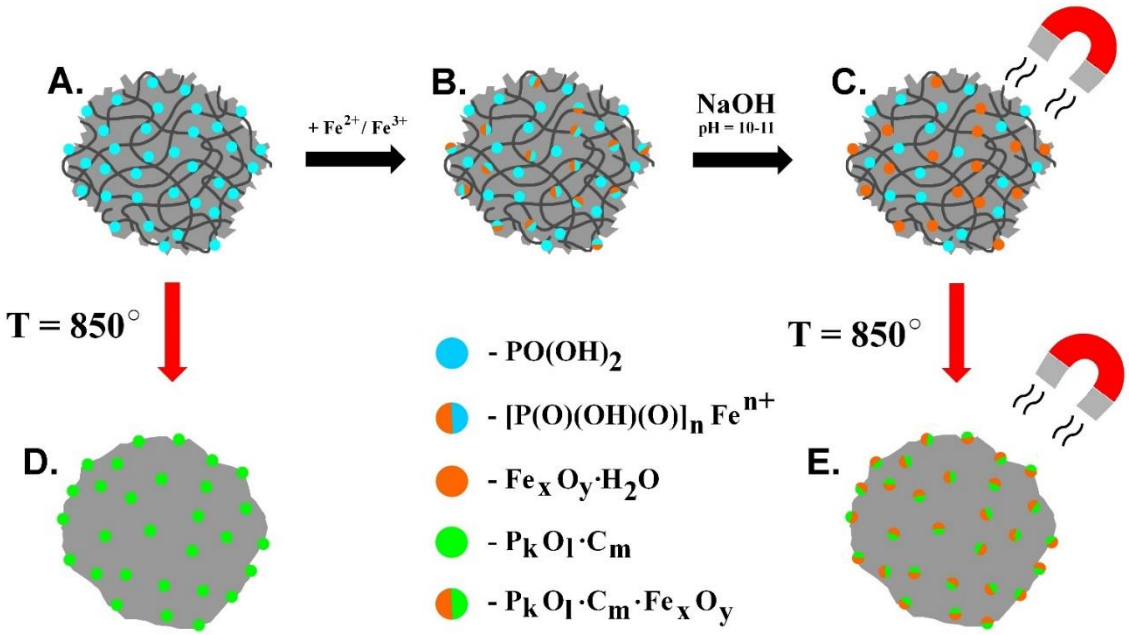

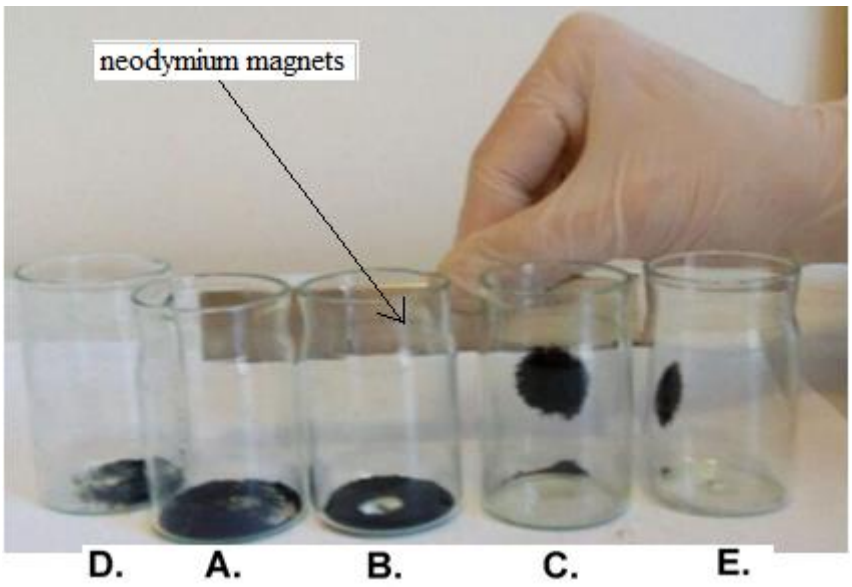

Figure 1. Schematic presentation of the preparation of the Ph-MNC from PhCP, their calcination and real illustration of magnetic properties: A. PhCP, B. PhCP with adsorbed iron ions, C. Ph-MNC, D. calcinated PhCP (C-PhCP), E. calcinated Ph-MNC (CPh-MNC).

Figure 2. The photograph showing the recovery of MNC form its suspension by application of external magnetic field (neodymium magnets).

3.1. X-ray diffraction studies

Ph-MNC was found to have a generally amorphous structure as it was shown using XRD (see Fig. 3). The observed diffraction peaks at (1.1.1), (2.0.0), (2.2.0), (4.2.2) and (5.1.1) agree well with the structure of magnetite (Fe_3O_4). Along with these diffraction peaks at (1.0.4), (2.2.2), (1.1.3), (1.2.2) and (2.1.4) attributed to hematite (α-Fe_2O_3). In addition of the peaks of

magnetite and hematite some peaks of goethite (FeO(OH), 1.1.0) and maghemite (γ-Fe_2O_3, 3.1.1) were also found in the prepared nanocomposite [40,41,42]. While the synthetic methods employing both Fe^{3+} and Fe^{2+} ions should lead to formation of magnetite the presence of other forms of iron oxide cannot be excluded as e.g. magnetite and maghemite form crystallographically isomorphous spinel structure. Moreover, magnetite very slowly oxidizes to maghemite at ca. room temperature [43]. XRD-based identification of a particular iron oxide in nano-sized particles is difficult because of significant peak broadening due to the size effect. It is also known that the hydrolysis of acidic solutions of iron salts can result in various iron oxides and oxohydroxides, depending on the reaction conditions. The fast hydrolysis of Fe^{3+} solution typically leads to amorphous non-stoichiometric hydrated oxohydroxide $Fe_2O_3 \cdot nH_2O$, which is also known as ferrihydrite [44]. Nevertheless, the presence of various types of iron oxides does not reduce the value of the resulting composite as almost all of them may also serve as absorbents [45].

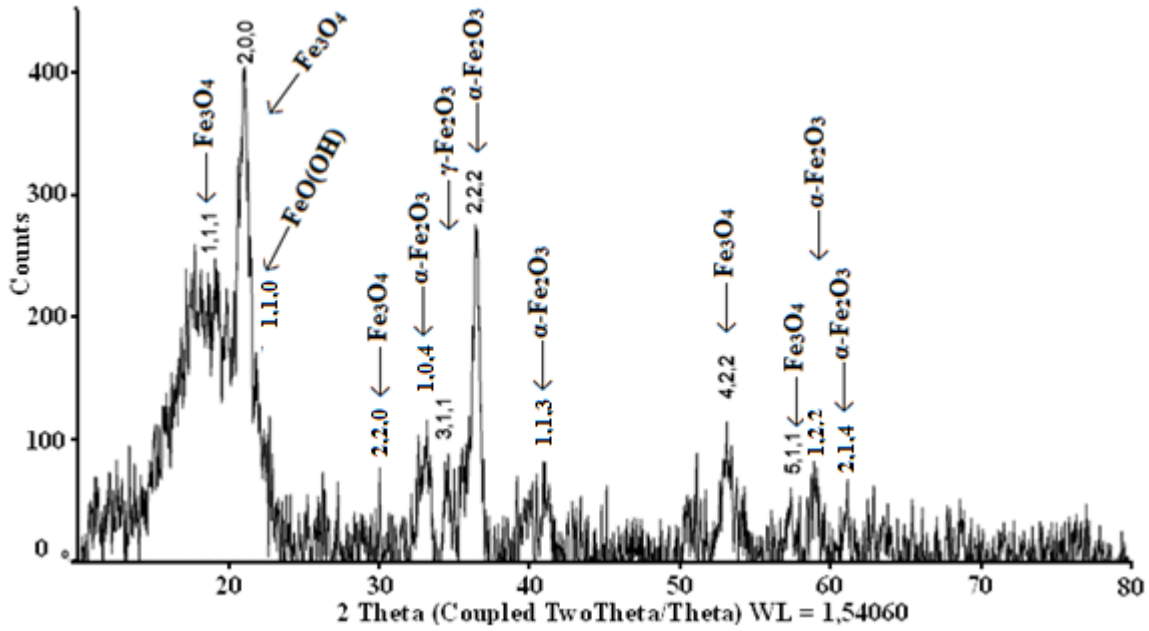

Figure 3. XRD patterns of Ph-MNC nanocomposite.

3.2. Comparative structural characteristics of PhCP and Ph-MNC

3.2.1. FT-IR analysis of PhCP and Ph-MNC

The FT-IR spectra of the PhCP and Ph-MNC are shown in Fig. 4. In the spectrum of PhCP the IR bands in 1200–1150 cm^{-1} region can be assigned to –P=O groups vibrations. The IR bands at 1702, 2864 and 3394 cm^{-1} are attributed to OH vibration in $–PO(OH)_2$ groups. IR band at 986 cm^{-1}, corresponding to C–O–P bond, indicates the attachment of $–PO(OH)_2$ group to the polymer chain *via* oxygen [38].

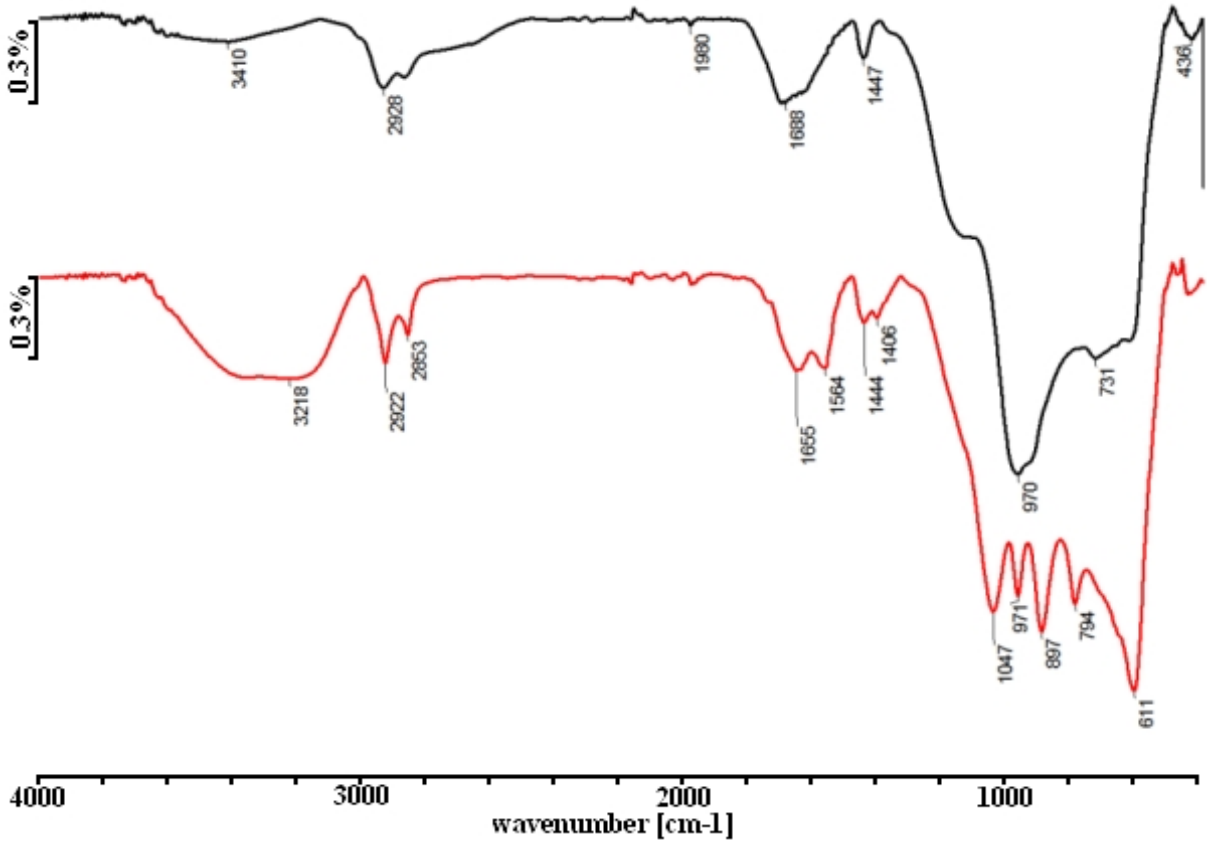

Figure 4. The FT-IR transmission spectra of the PhCP (black) and Ph-MNC (red).

Comparison of the of PhCP and Ph-MNC spectra indicates significant differences in the regions of 400-1100 and 3000-3600 cm^{-1}. While characteristic absorption bands of the Fe–O bond of iron oxides (mainly in magnetite and maghemite) are reported to be located between 400 and 700 cm^{-1} [46,47]. The band of the Fe–O bond in bulk iron oxides that is located at 570 cm^{-1} [48] was shifted in the nanocomposite system to higher wave numbers (611 cm^{-1}) that is common for iron oxide NPs [49]. Besides this, the data also reveal that the presence of characteristic IR band at ~1047 cm^{-1}, corresponding to inner-sphere Fe–O–P bonds [50]. This

band indicates that the iron oxide particle in Ph-MNC may be covalently bond *via* surface hydroxyl groups to polymeric phosphorous containing groups. The sharp bands located at 794 and 897 cm^{-1}can be assigned to the vibrations of the free –OH groups on the surface of the iron oxide particles. Moreover, differences between the spectra of PhCP and Ph-MNC in the region of 3000-3600 cm^{-1} can be explained by the same reason. The broad band in the region of 3300-3600 cm^{-1} can be also attributed to water adsorbed on the iron oxide particles [51].

3.2.2. Identification of thermal decompositions steps of PhCP and Ph-MNC

TG curves for PhCP and Ph-MNC samples are shown in Fig. 5. The degradation stages and the weight losses, at various heating rates, derived from the TG curves are listed in Table 1.

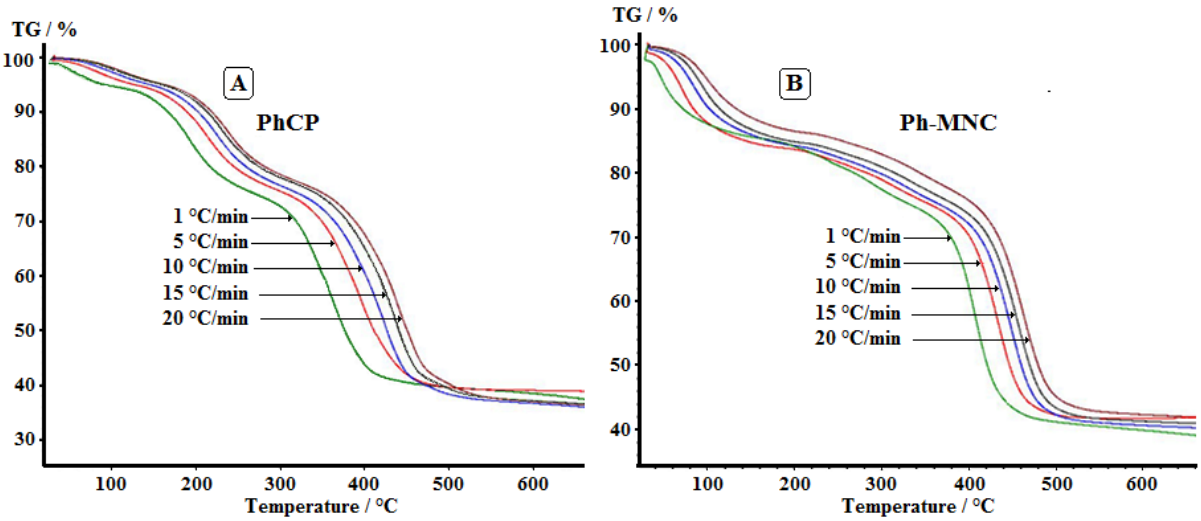

Figure 5. TG curves of the PhCP (A) and Ph-MNC (B) with different heating rates.

The degradation of the samples proceeds in general three stages. Visual inspection of the plots of samples and values of weight loss shows that degradation of the PhCP and the Ph-MNC proceed differently. This difference is clearly visible in the first two stages of degradation. The temperature range the first stage is between ca. 30 and 160°C and the average weight loss is equal to 4.3 wt.% for the PhCP. Based on the experimental condition (synthesis, pre-treatment procedure) and structure of the samples (porous and cross-linked),

weight loss at this stage is due to elimination of physically adsorbed water existing in the pores and of the hydrogen-bonded water with the functional groups. The first stage for Ph-MNC was recorded in wider temperature range (30–210°C) in comparison to PhCP. The values of weight loss for the composite were more than 3 times larger (Table 1, 11÷15 w/w. %). This fact may be explained by the presence of magnetic NPs in the pores and on the surface of PhCP. Magnetic NPs possess hydroxyl groups in their structure that may bound additional water molecules.

Table 1. Mass change and characteristic temperature of thermal degradation for PhCP and Ph-MNC at different heating rate.

Samples	Heat rate, K	Mass, mg	First step				Second step				Third step				Residue at 850°C
			T_i	T_m	T_f	Δm, %	T_i	T_m	T_f	Δm, %	T_i	T_m	T_f	Δm, %	%
PhCP	1	10.365	36	44	105	4.2	105	194	274	19.8	274	365	500	35.2	26.5
	5	10.332	36	83	129	4.4	129	214	294	19.1	294	353	560	36.8	36.3
	10	10.356	36	102	140	4.5	140	226	306	19.1	306	424	580	39.3	31.5
	15	10.428	36	108	149	4.4	149	232	313	18.3	313	436	590	40.0	33.0
	20	10.050	36	113	156	4.6	156	238	319	18.0	319	442	600	40.4	32.8
Ph-MNC	1	10.337	36	45	160	11.7	160	290	325	9.8	325	407	500	34.4	35.2
	5	10.340	36	70	186	14.6	186	313	345	8.1	345	434	560	34.0	43.0
	10	10.246	36	84	201	15.0	201	329	358	8.5	358	448	580	34.9	39.0
	15	9.887	36	93	206	14.8	206	338	368	8.6	368	456	590	34.8	39.9
	20	10.089	36	101	210	13.4	210	346	372	8.4	372	463	600	35.6	40.8

T_i – initial degradation temperature, °C
T_m – temperature corresponding to the maximum rate of degradation, °C
T_f – final degradation temperature, °C

The final degradation temperature of the second stage is in the ranges of 274–319°C, and 325–372°C for PhCP and Ph-MNC, respectively. This stage is characterized by a large change on TG curve slopes for PhCP, while for Ph-MNC this segment is different. Those results were also confirmed by roughly twice larger weight loss for PhCP (18÷20 w/w. %) than the one observed for Ph-MNC (8÷10 w/w. %). This step of thermal degradation may be

assigned to dehydration processes, anhydridization of phosphonate and phosphate groups and elimination of hydrogen chloride. The products of the degradation process may interact with magnetite particles, so the weight loss of the composite is less than that of the sole polymer.

At higher temperatures the third weight loss stage for both samples is characterized by a sharp change on TG curve slopes, especially in the case of Ph-MNC. The weight loss increases similarly for both materials reaching the average level of 37.0±3.0 %. This stage could be attributed to elimination of side groups from the polymer chains, random depolymerization and detachment of larger organic molecules that could be formed in the second stage. At such high temperatures cracking and gasification processes occur as well. The obtained results show that magnetic NPs do not significantly affect the values of weight loss at the third degradation stage indicating that the particles do not react with the degradation products or newly formed intermediate compounds decompose again. Finally, the residual amounts of the samples were compared. The mass of residue for Ph-MNC was ca. 7-9% (with respect to the starting masses) higher than for PhCP that is in good agreement with the amount of iron in the composite determined before thermal degradation (6 %).

3.3. Kinetics of the thermal degradation of PhCP and Ph-MNC

According to non-isothermal kinetic theory, TD of polymers can be expressed by the following equation (1):

$$\frac{d\alpha}{dT} = \frac{1}{\beta} A e^{\frac{-E_a}{RT}} f(\alpha) \qquad (1)$$

where $f(\alpha)$ is the differential expression of a kinetic model function, α is the fractional mass loss, β is heating rate, E_a and A are the so-called activation energies and pre-exponential factor for the decomposition reaction, respectively, R is the general gas constant. The fractional mass loss is a measure of reaction progress as a function of time or temperature. For non-isothermal TGA, the fractional mass loss can be calculated with a formula (2):

$$\alpha = \frac{m_0 - m_T}{m_0 - m_\infty} \qquad (2)$$

Where, m_0 is the initial sample weight, m_T is the sample weight at temperature T, and m_∞ is the final sample weight.

In the study for evaluation of kinetic parameters (E_a, A) OFW [52−54] and Friedman [55] methods were chosen. These methods can be successfully used to study TD kinetics for polymers, blends and composites, without any a'priori knowledge of the reaction mechanism. The kinetic parameters were calculated using a Netzsch Thermokinetics Software [56]. The mean values of E_a and A for the studied samples are presented in Table 2.

Table 2. The kinetics parameters obtained by Friedman and OFW methods for PhCP and Ph-MNC.

Sample	Step I				Step II				Step III			
	E_a, kJ·mol^{-1}		A, s^{-1}		E_a, kJ·mol^{-1}		A, s^{-1}		E_a, kJ·mol^{-1}		A, s^{-1}	
	Friedman	OFW	Friedman	OFW	Friedman	OFW	Friedman	OFW	Friedman	OFW	Friedman	OFW
PhCP	62	64	$2.9\cdot10^7$	$2.8\cdot10^7$	131	125	$1.5\cdot10^{11}$	$7.7\cdot10^{10}$	142	143	$2.0\cdot10^8$	$3.6\cdot10^8$
Ph-MNC	66	69	$3.4\cdot10^7$	$3.4\cdot10^7$	153	143	$2.7\cdot10^{11}$	$6.5\cdot10^{10}$	233	232	$3.9\cdot10^{14}$	$4.9\cdot10^{14}$

Values of kinetic parameters calculated by the two methods (see Table 2) for the first degradation stage are very similar for both materials. The overall E_a of the first degradation stage was found to be in the range 60-70 kJ mol^{-1}. Kinetic parameters values of the second thermal degradation stage are higher than for the previous stage. E_a of PhCP was 131, 125 kJ mol^{-1} and that of Ph-MNC was equal to 153, 143 kJ mol^{-1}, based on Friedman and OFW methods, respectively. This indicates that the presence of magnetic NP in the composite influences E_a likely due to larger problems with removal of the decomposition products from

the reaction medium. This effect becomes more pronounced in the third stage of degradation process. E_a for the composite is almost 100 kJ mol^{-1} higher than for PhCP.

Thus, during the TD process significant change associated with structure of the samples takes place in the second and third stages. Therefore, to have a more complete image of the thermal behavior of the studied samples, the variation of E_a vs α during the second and third degradation stages was plotted in Figure 6. Comparison of the E_a vs. α plot in Fig. 6 leads to conclusion that the second stage is the crucial degradation process for the samples because it is non-stationary in non-isothermal conditions. By increasing the temperature the continuous increase of E_a was observed for the second stage. The results also show that the E_a–α plot for the composite differ from the corresponding plot of PhCP (compare the slopes). Thus, magnetic NP seem to change the mechanism of the polymer degradation.

The variations of E_a taking place in the third degradation stage are plotted in Fig. 6B. The E_a values for both samples exhibit sinusoidal variation with α indicating changes in the degradation pathway. In this degradation stage, the decrease of E_a (in the range $0.35<\alpha<0.8$) could be also caused by the loss of the degradation products formed by the rupture of the functional groups attached to the polymer backbone. This variation of E_a, characterized by a dramatic increase or decrease as a function of α could be assigned either to some competitive processes or to the depolymerization in non-stationary conditions.

Finally, by comparison of the E_a–α plots obtained by the two applied methods very similar behavior was observed in the second and third stages. Thus, it would appear that either the differential (Friedman) or integral (OFW) method can provide a satisfactory mathematical approach to establishing the kinetic parameters for the thermal degradation of functional polymer as well as the studied composite.

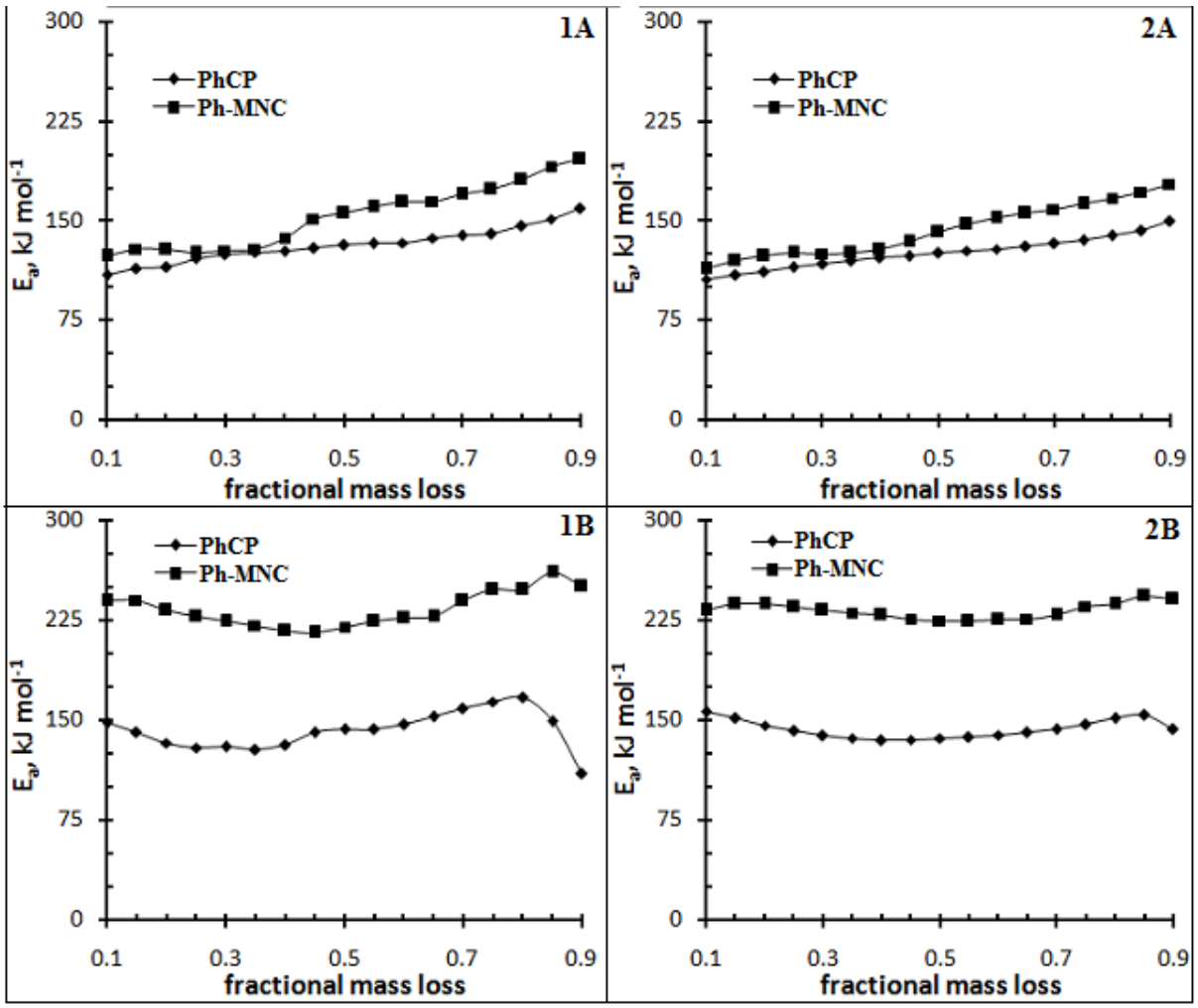

Figure 6. Variation of E_a versus fractional mass lose (α) for the second (A) and third (B) degradation stages of samples based on Friedman (1) and OFW (2) methods.

3.4. FTIR analyses of the calcinated polymer and nanocomposite

To make it clear how the presence of magnetic NP influences TD process the calcinated polymer (C-PhCP) and composite (C-Ph-MNC) were investigated and compared. In the spectrum of C-PhCP (see Fig. 7) the peaks corresponding to –CH_2– (2928 cm^{-1}), –CH– (2851 cm^{-1}), C–O–C (1090 cm^{-1}) groups as well as the bands attributed to phosphorus oxide in the range of 700-1000 cm^{-1} [57] were observed. In the spectrum of the C-Ph-MNC except the peaks corresponding to phosphorus oxide and iron oxide the other bands have vanished. This result can be explained by the catalytic effect of the iron oxide. According to the literature

nanosized transition metallic oxides such as iron oxide, magnetite, hematite, and maghemite are materials that may play a role of catalysts in thermal degradation reactions [58].

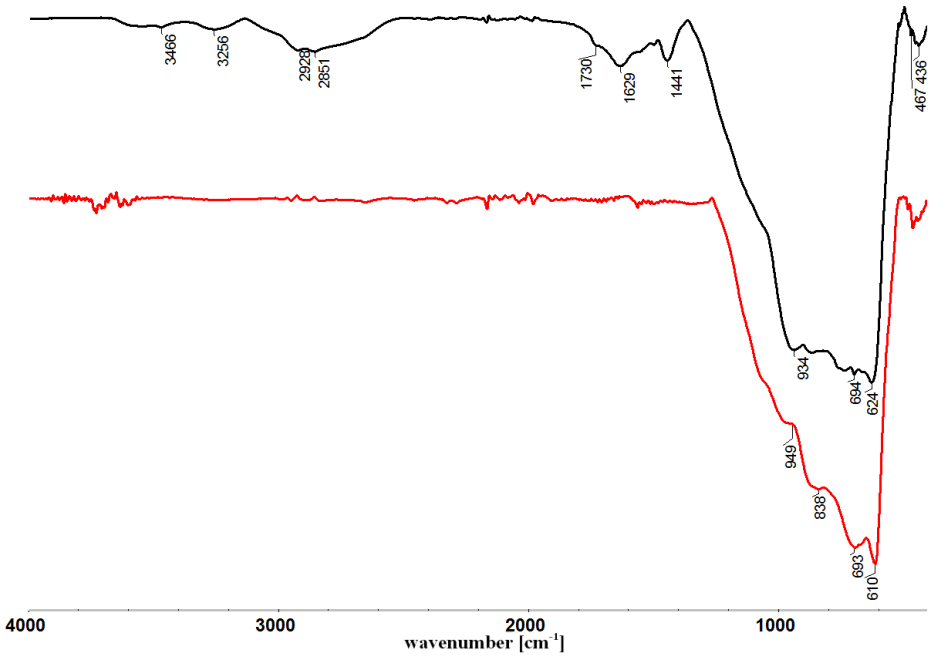

Figure 7. The FT-IR spectra of the C-PhCP (black) and C-Ph-MNC (red).

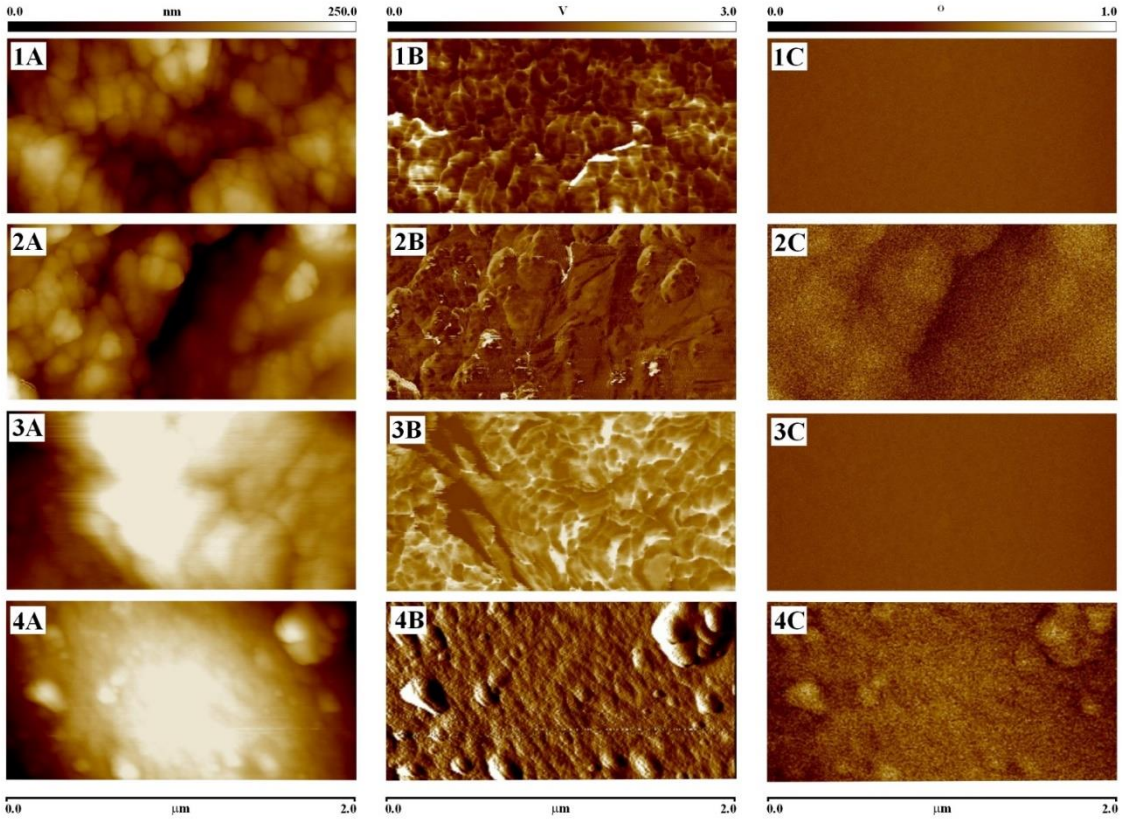

Figure 8. AFM images of topography (A), mechanical phase (B) and MFM (magnetic) phase (C) for: 1 - PhCP, 2 - Ph-MNC, 3- C-PhCP, 4 - C-Ph-MNC.

3.5. AFM-MFM characterization of PhCP, Ph-MNC and their calcinated forms

MFM was used to confirm magnetic properties of the obtained structures and determine the size of the magnetic particles (see Fig. 8). The microscope worked in the interleave mode which allowed to obtain AFM topography and phase images as well as MFM magnetic phase image form exactly the same areas on the sample. Only the samples with incorporated magnetic particles (Ph-MNC, C-Ph-MNC**)** revealed signal in the MFM phase images. It can only be observed for the samples possessing magnetic domains which are able to interact with the magnetized tip. That clearly indicates that the investigated nanocomposite samples exhibit strong magnetic properties and the distribution of the particles is relatively uniform. Samples without magnetic NPs (PhCP, C-PhCP) even they are characterized by nanostructured surface (see Fig. 8 1A and 8 3A) do not exhibit any magnetic properties (see Fig. 8 1C and 8 3C).

Differences in topography between initial samples (before calcination) and its calcinated forms were studied using AFM. The biggest differences were observed for the same types of material before and after thermal treatment. The surfaces of samples after the treatment became significantly smoother (see Fig. 9.)

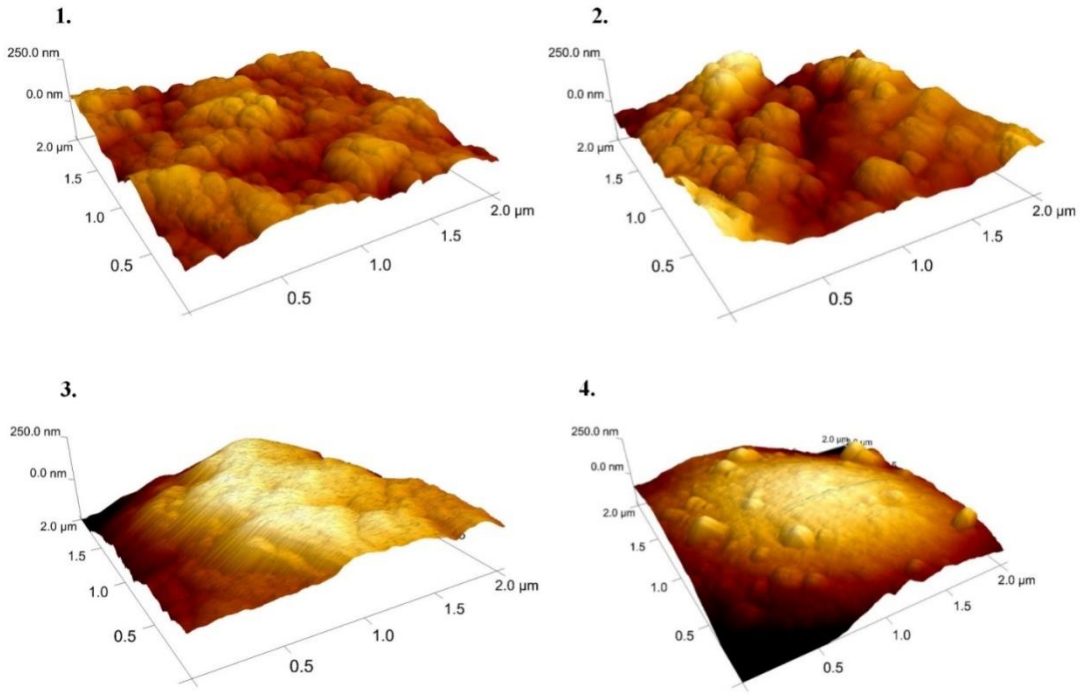

Fig. 9. 3D AFM topography images of: 1- PhCP, 2- Ph-MNC, 3- C-PhCP, 4- C-Ph-MNC.

4. Conclusions

A magnetic nanocomposite (Ph-MNC) was synthesized based on inexpensive phosphorus-containing polymer (PhCP) in a facile process by formation of iron oxide nanoparticles in the polymer matrix from the soluble precursors. The presence of functional groups, porous structure and the rough surface of the polymer allowed adsorption of iron ions from solution followed by formation of P-O-Fe bonds. Subsequent treatment with sodium hydroxide lead to formation of magnetic nanoparticles within the polymer matrix. FTIR data proved that the composite containing iron containing compounds was formed while XRD data indicated the presence of particles in the form of magnetite, maghemite, goethite, hematite and ferrihidrite. AFM studies enabled determination of sizes of the nanoparticles to be in the range ca. 100-160 nm that also showed strong magnetic properties as mapped using MFM.

Thermal degradation of the nanocomposite was studied using TGA. The obtained TG curves clearly showed the presence of three degradation stages for both PhCP and Ph-MNC. It was found that the first stage of weight loss covers a wider temperature range and the values of weight loss were more than three times larger for Ph-MNC as compared to PhCP likely due to the presence of hydroxyl groups on the surface of magnetic particles that linked more water molecules. However, the weight loss in the second stage was for Ph-MNC roughly twice smaller than for PhCP as magnetic NPs can interact stronger with the products of degradation at this stage (e.g. water, HCl). At higher temperatures (above 270°C) the third weight loss stage characterized by a steep slope in TG curves and almost the same weight loss for both samples was observed. It indicates that magnetic NPs do not react with the degradation products at this stage or the interactions lead to products that at such temperatures subsequently decompose. Kinetic parameters, such as E_a and A values were calculated according to Friedman and OFW methods. The comparison of the plots of E_a versus fractional mass loss for the second and third stages of PhCP and Ph-MNC indicate that the magnetic NPs strongly influence the complex degradation mechanism of the nanocomposite.

The native and calcinated nanocomposites (C- Ph-MNC) were shown to exhibit strong magnetic properties due to the presence of uniformly distributed NPs as evidenced using AFM and MFM. Thus, thermal degradation of the studied nanocomposite may be considered as a method for obtaining phosphorus-containing magnetic materials that may be of high application potential as magnetically separable sorbents. The presented result indicate that thermal treatment may be also used for regeneration of used magnetic nanocomposites.

Acknowledgement

The authors would like to thank to a Science Development Foundation under the President of the Republic of Azerbaijan and German Research Center for Environmental Health, Helmholtz Zentrum München, Joint Mass Spectrometry Centre, Cooperation Group ″Comprehensive Molecular Analytics″ for financial support. Part of research was done when R. Alosmanov joined the group of prof. S. Zapotoczny under Erasmus Mundus Electra program (financed by the Europeran Union). The authors would like to thank Gülcin Abbaszade and Karol Wolski for their help in measurements.

References

[1] Stark W J, Stoessel P R, Wohlleben W and Hafner A 2015 Industrial applications of nanoparticles *Chem. Soc. Rev.* **44** 5793–805

[2] Joo S H and Zhao D Y 2017 Environmental dynamics of metal oxide nanopatricle in heterogeneous systems: A review *J. Hazard. Mater.* **322** 29−47

[3] Song Y H, Li Y H, Xu Q and Liu Z 2017 Mezoporous silica nanoparticles for stimuli-responsive controlled drug delivery: advances, challenges, and outlook *Inter. J. Nanomed.* **12** 87−110

[4] Kinge S, Crego-Calama M and Reinhoudt D N 2008 Self-assembling nanoparticles at surfaces and interfaces *Chemphyschem* **9** 20−42

[5] Schmid G 2004 Nanoparticles: From Theory to Application (New York: Wiley Interscience)

[6] Wang Y, Guo J, Li L, Ge Y, Li B and Zhang Y 2017 High-loading Fe_2O_3/SWNT composite films for lithium-ion battery applications *Nanotechnology* **28** 345703

[7] Liu Y, Liu B and Nie Z 2015 Concurrent self-assembly of amphiphiles into nanoarchitectures with increasing complexity *Nano Today* **10** 278−300

[8] Balazs A C, Emrick T and Russel T P 2006 Nanoparticle Polymer Composites: Where Two Small Worlds Meets *Science* **314** 1107−10

[9] Nicolais L and Carotenuto G 2005 Metal-Polymer Nanocomposites (New York, Wiley Interscience)

[10] Ma J, Hu J M, Li Z and Nan C W 2011 Recent Progress in Multiferroic Magnetoelectric Composites: from Bulk to Thin Films *Adv. Mater.* **23** 1062−87

[11] Coemy J M D 1999 Whither magnetic materials? *J. Magn. Magn. Mater.* **196−197** 1−7

[12] Novakova A A et al. 2003 Magnetic properties of polymer nanocomposites containing iron oxide nanoparticles. *J. Magn. Magn. Mater*. **258** 354−357.

[13] Szpak A, Kania G, Skórka T, Tokarz W, Zapotoczny S and Nowakowska M 2013 Stable aqueous dispersion of superparamagnetic iron oxide nanoparticles protected by charged chitosan derivatives. *J. Nanoparticle Res.* **15** 1372−83

[14] Kania G et al. 2018 Uptake and bioreactivity of charged chitosan-coated superparamagnetic nanoparticles as promising contrast agents for magnetic resonance imaging *Nanomedicine* **14** 131−40

[15] Xu C, Zhang C, Wang Y, Li L, Li L and Whittaker A K 2017 Controllable synthesis of a novel magnetic core-shell nanoparticle for dual-modal imaging and pH-responsive drug delivery *Nanotechnology* **28** 495101

[16] Kesavan M P et al. 2017 Magnetic iron oxide nanoparticles (MIONs) cross-linked natural polymer-based hybrid gel beads: Controlled nano anti-TB drug delivery application. J. Biomed. Mater. Res. Part A. DOI: 10. 1002/jbm.a.36306

[17] Hervault A, Thanh N T 2014 Magnetic nanoparticle-based therapeutic agents for thermochemotherapy treatment of cancer *Nanoscale* **6** 11553–73.

[18] Mornet S, Elissalde C, Bidault O, Weill F, Sellier E, Nguyen O and Maglione M 2007 Ferroelectric-based nanocomposites: toward multifunctional materials *Chem. Mater.* **19** 987−92

[19] Alguero M et al. 2014 Thin Film Multiferroic nanocomposites by ion Implantation *ACS Appl. Mater. Interfaces* **6** 1909−15

[20] Menini L, Pereira M C, Ferreira A C, Fabris J D and Gusevskaya E V 2011 Cobalt–iron magnetic composites as heterogeneous catalysts for the aerobic oxidation of thiols under alkali free conditions *Appl. Catal. A: General* **392** 151–7

[21] Leung K C, Sham K W, Chak C P, Lai J M, Lee S F, Wang Y X and Cheng C H 2015 Evaluation of biocompatible alginate- and deferoxamine-coated ternary composites for magnetic resonance imaging and gene delivery into glioblastoma cells *Quant. Imaging Med. Surg.* 5 382–91

[22] Cho D-W, Jeon B-H, Chon C-M, Schwartz F W, Jeong Y and Song H 2015 Magnetic chitosan composite for adsorption of cationic and anionic dyes in aqueous solution *J. Ind. Eng. Chem.* **28** 60−6

[23] Kalia S, Kango S, Kumar A, Haldorai Y, Kumari B and Kumar R 2014 Magnetic polymer nanocomposites for environmental and biomedical applications *Colloid Polym. Sci.* **292** 2025–52

[24] Zapotoczny S, Szczubiałka K and Nowakowska M 2015 Nanoparticles in endothelial theranostics *Pharmacol. Rep.* **67** 751–5

[25] Gubin S P, Koksharov Y A, Khomutov G B and Yurkov G Y 2005 Magnetic nanoparticles: Preparation, structure and properties *Russ. Chem. Rev.* **74** 489–520

[26] Behrens S and Appel I 2016 Magnetic nanocomposites *Curr. Opin. Biotechnol.* **39** 89–96

[27] Sun Z, Zhou X, Luo W, Yue Q, Zhang Y, Cheng X, Li W, Kong B, Deng Y and Zhao D 2016 Interfacial engineering of magnetic particles with porous shells: Towards magnetic core –porous shell microparticles *Nanotoday* **11** 464–82

[28] Liu C, Qu C, Wang D, Feng H, Liu P and Zhang Y 2015 Preparation and characterization of magnetic polyimide composite films copolymerized with aminophthalocyanine-coated Fe_3O_4 nanocrystals *J. Mater. Sci: Mater. Electron.* **26** 4005–14

[29] Dong S, Xu M, Wei J, Yang X and Liu X 2014 The preparation and wide frequency microwave absorbing properties of tri-substituted-bisphthalonitrile/Fe_3O_4 magnetic hybrid microspheres *J. Magn. Magn. Mater.* **349** 15−20

[30] Ziolo R F, Giannelis E P, Weinstein B A, Ohoro M P, Ganguly B N, Mehrotra V, Russell M W and Huffman D R 1992 Matrix-mediated synthesis of nanocrystalline gamma-Fe_2O_3 − a new optically transparent magnetic material *Science* **257** 219–23

[31] Sarkar S, Blaney L B, Gupta A, Ghosh D and SenGupta A K 2007 Use of ArsenXnp, a hybrid anion exchanger, for arsenic removal in remote villages in the Indian subcontinent *React. Funct. Polym.* **67** 1599–611

[32] Rodriguez A F R, Coaquira J A H, Santos J G, Silveira L B, Marmolejo E M, Trennenpohl W, Rabelo D, Oliveira A C, Garg V K and Morais P C 2009 Characterization of magnetite nanoparticles supported in sulfonated styrene-divinylbenzene mesoporous copolymer *Hyperfine Interact.* **191** 417−23

[33] Jacukowicz-Sobala I, Wilk Ł J, Drabent K and Kociołek-Balawejder E 2015 Synthesis and characterization of hybrid materials containing iron oxide for removal of sulfides from water *J. Colloid Interface Sci.* **460** 154–63

[34] Suber L, Foglia S, Ingo G M and Boukos N 2001 Synthesis, and structural and morphological characterization of iron oxide – ion-exchange resin and –cellulose nanocomposites *Appl. Organometal. Chem.* **15** 414–20

[35] Jacukowicz-Sobala I, Drabent K and Kociołek-Balawejder E 2015 Evaluation of ferromagnetic hybrid polymers obtained using cation exchangers *Mater. Chem. Phys.* **161** 107−15

[36] Jacukowicz-Sobala I, Ciechanowska A and Kociołek-Balawejder E 2014 Hybrid polymer containing ferric oxides obtained using a redox polymer. Part I. Synthesis and characterization *Polimery* **59** 131–5

[37] Alosmanov R M and Azizov A A 2012 Sorption isotherms of Nickel(II), Cobalt(II), Mercury(II), and Lead(II) ions on a phosphorus-containing polymeric sorbent *Russ. J. Inorg. Chem.* **57** 303–5

[38] Yilmaz E, Alosmanov R M and Soylak M 2015 Magnetic solid phase extraction of lead(II) and cadmium(II) on a magnetic phosphorus-containing polymer (M-PhCP) for their microsampling flame atomic absorption spectrometric determinations *RSC Adv.* **5** 33801−8

[39] Alosmanov R M, Azizov A A and Magerramov A M 2011 NMR Spectroscopic Study of Phosphorus-Containing Polymer Sorbent *Russ. J. Gen. Chem.* **81** 1477–9

[40] Ahn T, Kim J H, Yang H-M, Lee J W and Kim J-D 2012 Formation Pathways of Magnetite Nanoparticles by Coprecipitation Method *J. Phys. Chem. C* **116** 6069–76

[41] Karami H 2010 Synthesis and Characterization of Iron Oxide Nanoparticles by Solid State Chemical Reaction Method *J. Clust. Sci.* **21** 11–20

[42] Wu W, Wu Z, Yu T, Jiang C and Kim W 2015 Recent progress on magnetic iron oxide nanoparticles: synthesis, surface functional strategies and biomedical applications *Sci. Technol. Adv. Mater.* **16** 1–43

[43] Tang J, Myers M, Bosnick K A and Brus L E 2003 Magnetite Fe_3O_4 nanocrystals: spectroscopic observation of aqueous oxidation kinetics *J. Phys. Chem. B.* **107** 7501–6

[44] Schwertmann U and Cornell R M 2000 Iron Oxides in the Laboratory Second Edn (Wiley-VCH, Weinheim)

[45] Hua M, Zhang S, Pan B, Zhang W, Lv L and Zhang Q 2012 Heavy metal removal from water/wastewater by nanosized metal oxides: A review *J. Hazard. Mater.* **211–212** 317–31

[46] Ercuta A and Chirita M 2013 Highly crystalline porous magnetite and vacancy-ordered maghemite microcrystals of rhombohedralhabit *J. Cryst. Growth.* **380** 182–6

[47] Ma M, Zhang Y, Yu W, Shen H, Zhang H and Gu N 2003 Preparation and characterization of magnetite nanoparticles coated by amino silane *Colloid Surf. A* **212** 219–26

[48] Zayed M A, Ahmed M A, Imam N G and El Sherbiny D H 2016 Preparation and structure characterization of hematite/magnetite ferro-fluid nanocomposites for hyperthermia purposes *J. Mol. Liq.* **222** 895–905

[49] Hwang S W, Umar A, Dar G N, Kim S H and Badran R I 2014 Synthesis and Characterization of Iron Oxide Nanoparticle for Phenyl Hydrazine Sensor Applications *Sensor Lett.* **12** 1–5

[50] Suzuki T, Hashimoto H, Itadani A, Matsumoto N, Kunoh H and Takada J 2012 Silicon and phosphorus linkage with iron via oxygen in the amorphous matrix of Gallionella ferruginea stalks *App. Environ. Microbiology* **78** 236–41.

[51] Li Y S, Church J S and Woodhead A L 2012 Infrared and Raman spectroscopic studies on iron oxide magnetic nano-particles and their surface modifications *J. Magn. Magn. Mater.* **324** 1543–50

[52] Ozawa T A 1965 A new method of analyzing thermogravimetric data *Bull. Chem. Soc. Jpn.* **38** 1881–6

[53] Flynn J H and Wall L A 1966 A quick direct method for the determination of activation energy from thermogravimetric data *J. Polym. Sci. C Polym. Lett.* **4** 323–8

[54] Popescu C 1996 Integral method to analyse the kinetics of heterogeneous reactions under non-isothermal conditions. A variant on the Ozawa–Flynn–Wall method *Thermochim. Acta* **285** 309–23

[55] Friedman H L 1964 Kinetics of thermal degradation of char-forming plastics from thermogravimetry. Application to a phenolic plastics *J. Polym. Sci.* **6** 183–95

[56] NETZSCH-Thermokinetics 3.1 Software Help.

[57] Silverstein R M, Webster F X, Kiemle D J and Bryce D L 2014 Spectrometric Identification of Organic Compounds 8 edn

[58] Tudorachi N and Bunia I 2015 Synthesis and thermal investigation by TG–FTIR–MS analysis of some functionalized acrylic copolymers and magnetic composites with Fe_3O_4 *J. Anal. App. Pyrolysis* **116** 190–201